



The role of preferential evaporation on the ignition of multicomponent fuels in a homogeneous spray/air mixture

A. Stagni^{a,c,*}, L. Esclapez^c, P. Govindaraju^b, A. Cuoci^a, T. Faravelli^a,
M. Ihme^{b,c}

^a Department of Chemistry, Materials, and Chemical Engineering “G. Natta”, Politecnico di Milano, 20133 Milano, Italy

^b Department of Mechanical Engineering, Stanford University, Stanford, CA 94305, USA

^c Center for Turbulence Research, Stanford University, Stanford, CA 94305, USA

Received 3 December 2015; accepted 7 June 2016

Available online xxx

Abstract

This work examines the importance of preferential evaporation and liquid species diffusion on the ignition of multicomponent surrogate fuels in homogeneous mixtures. To this end, a model is developed that considers the evaporation of a monodisperse droplet cloud in a homogeneous and isobaric gas-phase environment. The mathematical model accounts for physico-chemical relevant processes, involving (i) species diffusion in the liquid phase, (ii) two-phase thermodynamic equilibrium and (iii) gas-phase chemistry. After evaluating the accuracy of individual model components against available experimental data, the model is applied to investigate the ignition of a surrogate mixture for a Jet-A fuel (POSF 4658) at conditions of interest to gas turbine engines. A parametric study is performed to examine effects on the interaction between multicomponent evaporation and ignition. It is found that the maximum reactivity occurs for conditions at which the ignition time in the gas phase is comparable to the evaporation time. At these conditions, the mixture composition is significantly affected by preferential evaporation, which in turn affects the reactivity of the gas phase. It is shown that intradroplet diffusion plays a major role on the radial droplet composition, thereby conditioning the evaporation rates of single species. A comparison with a zero-diffusivity model for the treatment of droplet internal diffusion emphasizes the importance of liquid diffusion on the autoignition time, and confirms the need for properly accounting for a detailed description of multicomponent evaporation effects.

© 2016 by The Combustion Institute. Published by Elsevier Inc.

Keywords: Droplets; Two-phase combustion; Preferential evaporation; Autoignition; Multicomponent diffusion

* Corresponding author at: Department of Chemistry, Materials, and Chemical Engineering “G. Natta”, Politec-

nico di Milano, 20133 Milano, Italy. Tel.: +39 02 2399 4716.

E-mail address: alessandro.stagni@polimi.it
(A. Stagni).

<http://dx.doi.org/10.1016/j.proci.2016.06.052>

1540-7489 © 2016 by The Combustion Institute. Published by Elsevier Inc.

1. Introduction

The use of surrogates to emulate the characteristic behavior of real fuels is an established methodology [1,2]. However, main topics of discussion have been on the selection of the set of species constituting the surrogate and the specific properties to be matched by a particular surrogate mixture. Ideally, physical (density, molecular weight, H/C ratio, viscosity, etc.) and chemical (ignition delay, flame propagation, soot formation, etc.) targets should be modeled to provide a comprehensive surrogate description. While few studies [3,4] have focused on both target properties, the main emphasis has been attributed to the description of the gas-phase behavior [5,6]. In fact, one of the main complexities in emulating real-fuel properties arises from the strong interaction between the liquid and the gas phase.

Constraining the surrogate formulation to meet specific targets does not imply a complete knowledge of its behavior. Combustion devices operate over a wide range of conditions, and the consideration of conditions that affect the two-phase interaction in combustion, such as temperature, pressure or droplet diameter, introduce a substantial degree of complexity if included in the fuel formulation. For instance, it is widely acknowledged [7] that the ignition delay time is one of the key properties to be reproduced by surrogate fuels. This property is usually contained in frameworks for the surrogate formulation through experimental measurements of the Derived Cetane Number (DCN) [8]. These measurements are carried out through a standardized procedure [9] at specific operating conditions, without providing direct control over specific droplet size distribution or local equivalence ratio. For these cases, an analysis of the influence of different parameters on the ignition delay time can be of primary importance to possibly further constrain a surrogate description.

Recently, particular attention has been devoted to the parametric analysis of the two-phase ignition behavior of different fuels. These studies have been carried out by considering idealized systems, such as spherical droplets in the absence of gravity to isolate chemical processes from other phenomena affecting combustion in real devices, as well as to make the problem computationally tractable using detailed kinetic mechanisms. While experimental [10] and computational [11–15] studies have focused on the ignition behavior of single-component droplets, less attention has been devoted to the investigation of multicomponent fuels. The description of multicomponent fuels requires the consideration of liquid-phase diffusion, non-ideal phase equilibrium, and extended chemical mechanisms for the description of multicomponent gas-phase chemistry. Although the importance of multicomponent evaporation on ignition has been recognized in automotive applications [16–18], the im-

portance for aviation fuels at gas-turbine-relevant conditions has not been considered so far. This is the subject of this work. Specifically, the objective of this study is to investigate effects of multicomponent diffusion and preferential evaporation on the ignition of fuel mixtures. To isolate these effects from the intricate coupling with the gas phase transport, arising in two-phase flow combustion, this study considers an idealized configuration in which the gas phase is represented by a semi-batch reactor. A numerical model is developed to represent the spatial evolution of the liquid phase inside monodispersed droplets, as well as the temporal evolution of the homogeneous gaseous phase. The model formulation is presented in Section 2, where each component of the model is validated. In Section 3, the model is applied to the analysis of the autoignition of the 2nd-generation surrogate of the POSF 4658 Jet-A fuel [8]. A parametric study of effects of droplet diameter and global equivalence ratio on evaporation and ignition is carried out, and the relevance of multicomponent evaporation is quantified through a comparison with a zero-diffusivity model. The manuscript finishes with conclusions.

2. Mathematical model

The mathematical model considers the evaporation and ignition of a monodispersed spray cloud in a homogeneous gas phase. To isolate the effect of preferential evaporation from transport in the gaseous mixture we consider the droplet evaporation into a homogeneous gas phase. Indeed, previous numerical studies showed that (i) in non-premixed systems, for low to moderate strain rates, ignition evolves in a manner comparable to that of homogeneous systems, but with slower dynamics because of diffusive losses [19]; and (ii) that in droplet cloud systems, compared to what is analyzed in this work, the ignition process tends to behave in a homogeneous way with decreasing droplet diameters [12]. Since our simulations consider both evaporation and gas-phase chemistry, ignition was considered either during evaporation or after evaporation is completed.

The following assumptions in the model formulation are made:

- Spherically symmetric and monodisperse droplets;
- Absence of chemical reactions in the liquid phase;
- Dynamic equilibrium with the underlying gas phase (no slip velocity);
- Constant pressure;
- Equilibrium conditions at the liquid/gas interface.

In the following subsections, the main model components are described.

2.1. Two-phase model

Conservation of species, energy and velocity in the droplet is solved by considering a spherically symmetric droplet [11]:

$$\rho_L \left(\frac{\partial Y_{L,i}}{\partial t} + v_L \frac{\partial Y_{L,i}}{\partial r} \right) = - \frac{1}{r^2} \frac{\partial}{\partial r} (r^2 j_{L,i}), \quad (1)$$

$$\rho_L c_L \left(\frac{\partial T_L}{\partial t} + v_L \frac{\partial T_L}{\partial r} \right) = \frac{1}{r^2} \frac{\partial}{\partial r} \left(r^2 k_L \frac{\partial T_L}{\partial r} \right) - \sum_i j_{L,i} c_{L,i} \frac{\partial T_L}{\partial r}, \quad (2)$$

$$\frac{\partial \rho_L}{\partial t} + \frac{1}{r^2} \frac{\partial}{\partial r} (r^2 \rho_L v_L) = 0, \quad (3)$$

where the subscript L refers to liquid-phase properties. ρ is the density, v is the convective velocity, Y_i is the mass fraction of the i th species, r is the radial coordinate, j is the diffusion flux, k is the thermal conductivity. $c_{L,i}$ and c_L are, respectively, the heat capacity of the i th species and of the mixture. The diffusion fluxes are described through Stefan–Maxwell theory [20]. For this purpose, the activity coefficients are evaluated using the UNI-FAC formulation [21]. Diffusion coefficients in the limit of infinite dilution are estimated through the Siddiqi–Lucas correlation [22] and binary diffusivities are estimated following Wesselingh and Krishna [20].

Due to spherical symmetry, boundary conditions at the droplet center require zero velocity for the liquid, and homogeneous Neumann conditions are prescribed for temperature and mass fractions. Interface properties are calculated from thermodynamic equilibrium, where the fugacity is evaluated through the Peng–Robinson equation of state, and mass and energy flux continuity. The resulting set of equations is discretized using an adaptive grid, with local adaptation near the droplet interface. In this work, 30 grid points were used to discretize the liquid phase, and previous work [11,14] shows that further grid refinement does not yield significant changes in the results.

The two-way coupling of the droplet with the 0D gas phase is based on an equilibrium law using the Spalding mass-transfer model [23]. The evaporation flux of species i and the heat flux at the droplet surface are evaluated following Bellan and Harstad [24], whose validity is supported by extensive benchmark cases [25]:

$$\phi_{s,i} = \frac{\dot{m}_{ev,i}}{4\pi r_d^2} = - \frac{1}{4\pi r_d^2} \frac{Sh_i m_d}{3Sc_i \tau_d} \ln(1 + B_{M,i}), \quad (4)$$

$$\phi_{s,T} = \frac{\dot{T}}{4\pi r_d^2} = \frac{1}{4\pi r_d^2} \left[\frac{Nuc_{p,G} f_2}{3Pr_L \tau_d} (T_G - T_{s,L}) + \frac{\sum_{i=1}^N \dot{m}_{ev,i} l_{v,i}}{m_d c_L} \right], \quad (5)$$

where the subscript s refers to the droplet surface conditions. m_d is the droplet mass and Sh_i , Sc_i and $B_{M,i}$ are the Sherwood number, the Schmidt number and the mass Spalding number of species i . The relaxation time of the droplet is $\tau_d = \bar{\rho}_L d_L^2 / (18\mu)$ with $\bar{\rho}_L$ being the average droplet density, d_L is the droplet diameter and μ is the dynamic gas viscosity. Nu is the Nusselt number, Pr is the Prandtl number and $l_{v,i}$ is the latent heat of evaporation of species i . f_2 is a correction factor to account for the Stefan flux in the interface heat balance.

The 0D semi-batch reactor equations for the gaseous species mass fractions and temperature are coupled to the liquid phase through the droplet number density n_L :

$$\frac{\partial \rho_G Y_{G,i}}{\partial t} = \dot{\omega}_i + n_L \delta_{i\{f\}} \dot{m}_{ev,i} \quad (6)$$

$$\frac{\partial \rho_G c_{p,G} T_G}{\partial t} = \dot{\omega}_T + n_L \left[c_L m_d \dot{T} + \sum_{i \in \{f\}} (c_{p,G,i} T_{L,s} \dot{m}_{ev,i} + l_{v,i} \dot{m}_{ev,i}) \right] \quad (7)$$

where $\delta_{i\{f\}}$ is the Kronecker delta function equal to 1 if i belongs to the liquid species ensemble $\{f\}$ and zero otherwise, $\dot{\omega}_i$ is the chemical source term of species i , $\dot{\omega}_T = - \sum_i h_i \dot{\omega}_i$ is the heat release rate with h_i the enthalpy of species i and $c_{p,i}$ is the constant-pressure specific heat of species i . The droplet number density n_L is related to the overall equivalence ratio Φ and the initial droplet diameter $d_{L,0}$ using $n_L = \Phi \rho_{air} s / m_{d,0}$ with s the stoichiometric fuel-air ratio.

2.2. Surrogate formulation

This study focuses on the conventional Jet-A POSF 4658 fuel blend, for which an extensive set of experimental data is available. A comprehensive approach for the formulation of the surrogate representation for transportation fuels was developed by Dooley et al. [8]. This approach is based on matching four combustion property targets of the corresponding real fuel: molecular weight, H/C ratio, Threshold Sooting Index (TSI), and DCN. Four species were selected as candidate components, namely n -dodecane, iso-octane, 1,3,5-trimethylbenzene and n -propylbenzene, representative of the three main classes of hydrocarbons present in a Jet-A fuel. Dooley et al. [8] found that the four target properties were matched by a mixture 40.4/29.5/7.3/22.8 (in molar fractions) of the mentioned species, which was then recommended as 2nd-generation fuel surrogate for POSF 4658. This surrogate representation was validated against a large set of experimental data, and is used as reference composition for the purposes of this work.

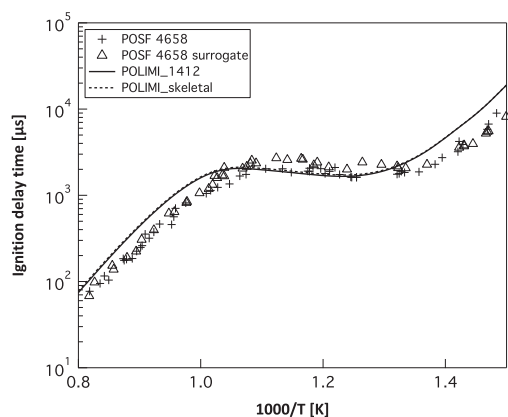


Fig. 1. Ignition delay times for the stoichiometric POSF 4658 fuel [7] and the 2nd-generation surrogate [8], compared to predictions obtained from the POLIMI mechanisms ($P = 20$ atm) [26,29].

2.3. Kinetic mechanism

The kinetic mechanism used for the description of the gas-phase chemistry is derived from the lumped model by Ranzi et al. [26], describing the pyrolysis, partial oxidation and combustion of hydrocarbons up to C_{16} and oxygenated fuels. To accelerate the calculations, the complete mechanism underwent a skeletal reduction procedure [27,28], following the numerical algorithm implemented in DoctorSMOKE++ [29]. For each surrogate component, a subset of important species was found by sampling a three-dimensional range of operating conditions ($T = 500 - 1700$ K, $P = 22.1$ atm, $\Phi = 0.25 - 2$) through adiabatic, constant-pressure batch reactors. A maximum error for the ignition delay time below 10% was set for each species, and a final mechanism of 181 species and 4089 reactions was obtained after merging the four subsets of component mechanisms (this mechanism is available as supplementary material).

Both detailed and skeletal mechanisms were utilized for predicting the ignition delay of the fully prevaporized 2nd-generation surrogate. Stoichiometric conditions were investigated [7,8] through shock tube and rapid compression machine experiments for both POSF 4658 fuel and the 2nd-generation surrogate. A constant-volume batch reactor was used to model the autoignition without pressure correction. Numerically, ignition was defined as the time when the maximum OH mass fraction occurred, and results are shown in Fig. 1. Considering the experimental uncertainty, as reported by Dooley et al. [8], and considering the ideal conditions of the 0D ignition model, good agreement between models and experiments is found. Moreover, these differences are coherent with results obtained by Vasu et al. [30] between shock tube exper-

iments for *n*-dodecane and the early mechanism by Ranzi et al. [26]. As a matter of fact, *n*-dodecane is the most abundant component of the surrogate, as well as the most reactive.

2.4. Thermodynamic and transport properties

Fuel descriptions usually contain compounds for which physical properties are not present in the existing literature. To describe the thermodynamic and transport properties of the liquid phase, a general method based on group contribution analysis [31] was proposed. In this method, critical conditions for pressure, temperature and volume, and acentric factors are calculated using functions which depend on linear contributions from each functional group. The evaluation of thermodynamic properties such as specific heat capacity, molar specific volume and latent heat of vaporization is then carried out by adding a second order correction, accounting for linear contributions from interactions between functional groups. To account for pressure and temperature dependencies, corrections are applied [21] considering the Peng–Robinson equation of state for gas and liquid density, Thodos correction for latent heat of vaporization, Wilke–Lee for low pressure vapor diffusion coefficients, Lee–Kesler correction for saturated vapor pressure, and the UNIFAC approach to estimate species activities.

Liquid properties are validated for POSF 4658 in idealized systems. The variation of the droplet diameter during evaporation is numerically reproduced and compared to experiments in Fig. 2a. The initial increase in diameter is due to a decrease in density with comparatively lower evaporation rate. Subsequently, the droplet diameter decreases according to the d^2 -law. A good agreement between experimental data and simulations for POSF 4658 fuel can be observed. The 2nd-generation surrogate mixture slightly underpredicts the total evaporation time. The distillation curve is then calculated, and data from advanced distillation measurements were used [32]. The experimental trend is bounded between the two asymptotic limits, i.e., flash and fractional distillation curves. These two limits are calculated using both real fuel mixture and surrogate, and comparisons are shown in Fig. 2b. Good agreement is obtained by the surrogate mixture, with the related flash curve being reasonably close to the one obtained from the full fuel description.

2.5. Implementation

The resulting large and stiff differential-algebraic (DAE) system is implemented by relying on the OpenSMOKE++ framework [34] for the liquid-grid discretization and the management of gas-phase kinetics, the BzzDAE library [35] for the DAE system solution and the

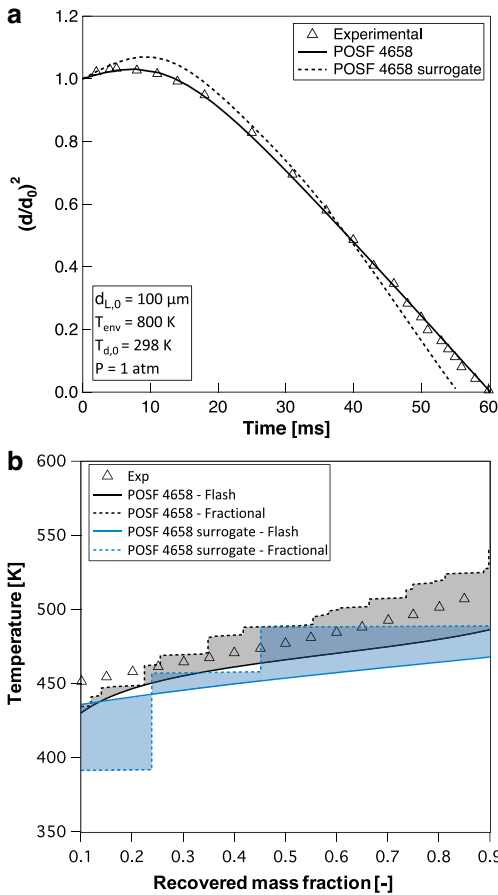


Fig. 2. (a) Comparison between experiments [33] and computed results for the evaporation of an isolated droplet. (b) Comparison between advanced distillation curve measurements [32] and predictions obtained through flash and fractional distillation calculations for POSF 4658 fuel and surrogate.

GroupContribution library [36] for the evaluation of liquid-phase thermodynamic and transport properties.

3. Autoignition of surrogate droplets in standard conditions

Using conditions for temperature and pressure prescribed in the DCN standard [9] ($T = 833$ K, $P = 22.1$ atm), the ignition delay time was calculated as a function of initial droplet diameter $d_{L,0}$ (10–100 μm) and global equivalence ratio Φ (0.5–2), i.e. in conditions usually found in gas turbine applications [37]. As an example of the temporal evolution of the droplet, the evolution of different species within the droplets is shown in Fig. 3 for the case with $d_{L,0} = 20$ μm and $\Phi = 1$. A significant difference can be observed between the composition at the center and at the interface, which is coherent with the relative volatility of the different species. For the conditions considered, the least volatile species is *n*-dodecane, whose evaporation rate is low at the beginning (Fig. 3a), in spite of being the most abundant species of the surrogate. The evaporation rate increases only when the mass fraction of *n*-dodecane approaches the value of unity near the surface. In contrast, iso-octane, i.e., the most volatile compound, evaporates at a significantly higher rate, eventually reaching a lower mass fraction than *n*-propylbenzene, which is present at a lower concentration. As a result, the gas-phase composition significantly changes over time. In these conditions, *n*-dodecane requires half of the droplet lifetime to become the prevailing fuel species in the gas phase despite being the controlling species for the ignition initiation.

The complete set of results is shown in the form of a contour map in Fig. 4, where ignition delay time τ_{ign} is considered as the time at which the temperature in the phase reaches its maximum slope.

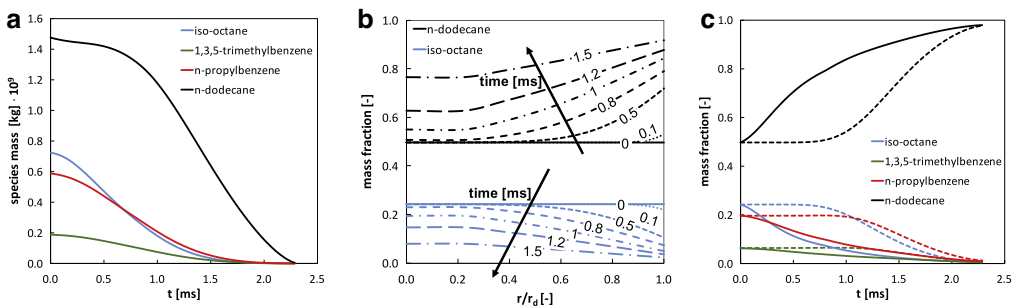


Fig. 3. Species profiles in a single droplet ($d_{L,0} = 20$ μm , $\Phi = 1$). (a) total liquid species mass over time, (b) normalized radial profile of *n*-dodecane and iso-octane over time, (c) center (dashed line) vs. interface (continuous line) mass fraction over time.

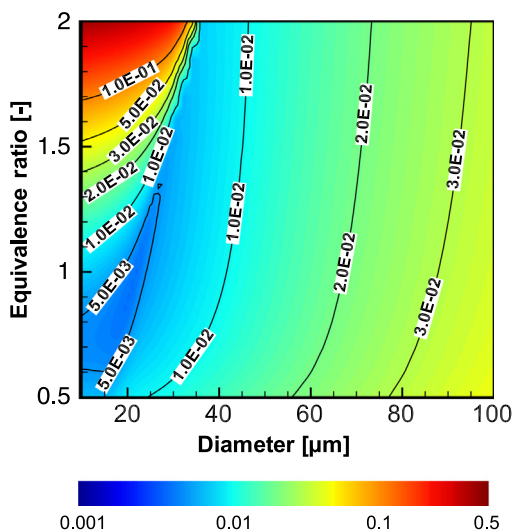


Fig. 4. Ignition delay times τ_{ign} [s] with finite diffusion for the 2nd-generation surrogate of POSF 4658.

The most reactive region is characterized by small droplet diameters and low equivalence ratios, and a minimum ignition delay is observed around $d_{L,0} = 20 \mu\text{m}$ and $\Phi = 0.8$. This minimum results from the non-monotonic behavior of both parameters under investigation. These trends are qualitatively similar to the results observed by Morieu et al. [12] for the autoignition of isolated droplets of *n*-heptane, and in simulations where both liquid and gaseous phase were spatially discretized. This indicates that the model proposed here is able to reproduce essential physical mechanisms to describe the competition between evaporation and ignition time scales.

In the present model, the droplet ignition delay is controlled by two main parameters: the availability of fuel and the gas temperature. Both are related to the evaporation process and thus influenced by the droplet size and number density (i.e., equivalence ratio). The classical picture proposed in the literature [38] is to consider that the ignition delay of the droplet cloud results from successive processes of evaporation and gaseous auto-ignition, so that the total ignition time can be approximated as $\tau_{ign} = \tau_{evap} + \tau_{pv,ign}$ where τ_{evap} and $\tau_{pv,ign}$ are the evaporation and autoignition time of the prevaporized mixture, respectively. For small droplet diameters where $\tau_{evap} \ll \tau_{pv,ign}$, this assumption holds and τ_{ign} is found to mainly depend on the equivalence ratio (region (i) in Fig. 5a). Indeed, for prevaporized mixtures, the heat extracted from the gas phase to achieve evaporation is directly proportional to the equivalence ratio. Due to the exponential dependence of $\tau_{pv,ign}$ with temperature (Fig. 1) a comparable exponential increase of τ_{ign} with Φ is observed. This effect is shown in Fig. 5a, where the difference between prevaporized ignition delay with and without heat losses by evaporation progressively increases from a factor two to two orders of magnitude with increasing Φ . For larger initial droplet diameters ($d_{L,0} > 40 \mu\text{m}$), τ_{ign} is limited by the fuel availability: with increasing equivalence ratio the ignition delay monotonically decreases as a result of the higher total evaporation rate. In this case, τ_{ign} can no longer be represented as the sum of evaporation and auto-ignition time of the gaseous mixture. At low equivalence ratios (region (iii) in Fig. 5a), its value is higher because of the low reactivity of the initially lean mixture. On the other hand, this trend is opposite at higher equivalence ratios (region ii), where the higher fuel availability allows for an earlier ignition.

Figure 5b shows that at the boundary between regions (i) and (ii) ignition is up to 100 times faster than the sum of τ_{evap} and $\tau_{pv,ign}$. Here, the sub-

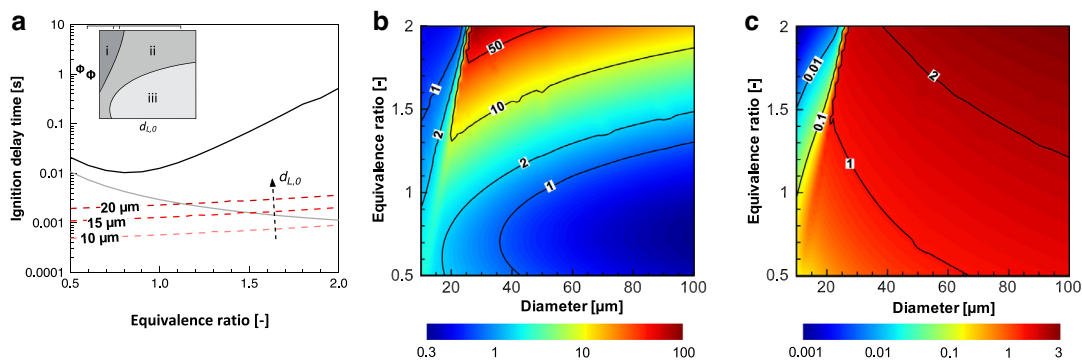


Fig. 5. (a) Ignition delay times of fully prevaporized mixture considering cooling effect (black full line) and without heat transfer by evaporation (gray full line). Evaporation time without combustion (dashed line). (b) $(\tau_{evap} + \tau_{pv,ign})/\tau_{ign}$ and (c) τ_{evap}/τ_{ign} ratios, where τ_{ign} was calculated with a constant-fuel composition (zero-diffusivity model).

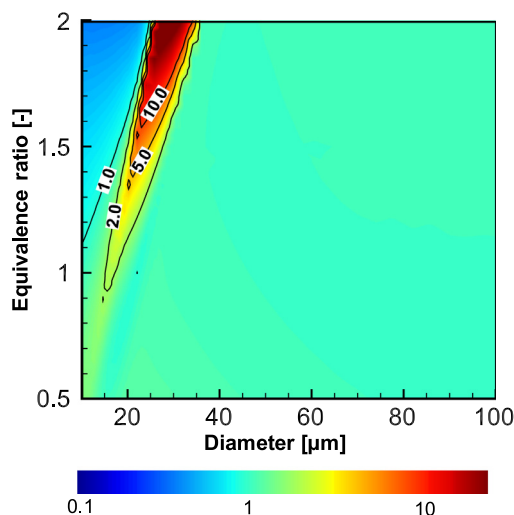


Fig. 6. Map of the ratio between droplet autoignition times, as calculated from finite diffusion model (Fig. 4) and zero-diffusivity model.

stantial equality between τ_{evap} and τ_{ign} , shown in Fig. 5c, makes this region more sensitive to preferential evaporation, which determines the composition of the evaporating mixture, and thus changes τ_{ign} . To further examine the importance of this composition, a comparison with a zero-diffusivity model is carried out. Because of the assumed zero diffusivity in the liquid phase, the composition of the evaporated mixture remains constant over the course of the evaporation. In numerical terms, this was approximated by multiplying all diffusion coefficients by a factor 0.001. The ratio between the autoignition times for the case with finite diffusion and the zero-diffusivity model is presented in Fig. 6. As predicted by the previous analysis, for large diameters no significant effects can be noticed. In contrast, important differences are evident in the left part of region (ii): here, the zero-diffusivity

model significantly underpredicts the autoignition time, and the ratio varies by a factor of two or more.

To better understand the variation of the ignition delay time in the zero-diffusion limit, the compositional variation of the surrogate mixture during the ignition process is evaluated. This is compared with the ignition delay of the corresponding prevaporized mixture for an initial condition of $T_0 = 833$ K and $P = 22.1$ atm. For the sake of clarity, the least abundant species (1,3,5-trimethylbenzene and *n*-propylbenzene) are combined. The result is shown in Fig. 7a for a mixture at 833 K, 22.1 atm and an overall equivalence ratio $\Phi = 1$. The vertices and edges of the triangle represent the pure compounds and binary mixtures, respectively. The *n*-dodecane is found to dominate the ignition behavior for most of the ternary mixtures. The trajectories superimposed on the gaseous composition space correspond to $d_{L,0} = 20$ μm and $\Phi = 1.0$, conditions for the finite-diffusion (triangle) and zero-diffusion (circle) cases. The trajectories are colored by the simulation time in order to highlight the time difference between both cases. The zero-diffusion limit is found to induce a significantly faster evaporation and higher content of *n*-dodecane resulting in a faster ignition. The subsequent rapid consumption of *n*-dodecane indicates that the ignition is driven by the high reactivity of the *n*-dodecane.

The corresponding temporal evolution of the gas phase is illustrated in Fig. 7b and c. Here, the different diffusion models give rise to a particularly interesting reactivity behavior: specifically, at the zero-diffusivity limit, the higher concentration of *n*-dodecane leads to an earlier low-temperature ignition. The evolution of the *n*-dodecane mole fraction results from the competition between oxidation and evaporation. The first maximum in *n*-dodecane (0.9 ms) is due to the initiation of the low-temperature ignition. Subsequently, since *n*-dodecane is affected by a Negative Temperature Coefficient (NTC) behavior (cfr. Fig. 1), its reactivity slows down and its concentration in-

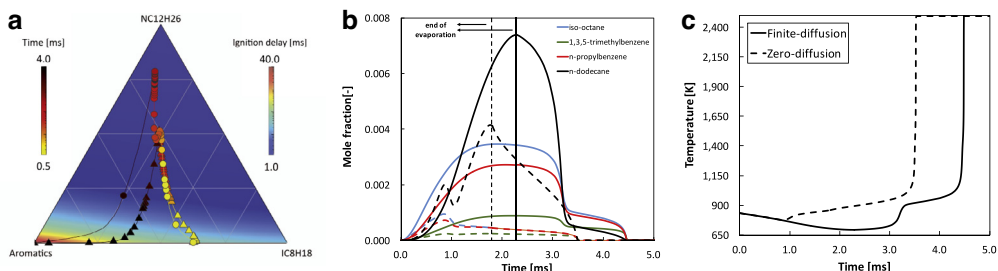


Fig. 7. Temporal evolution for $d_{L,0} = 20$ μm and $\Phi = 1$ ($P = 22.1$ atm, $T_0 = 833$ K). (a) Map of ignition delay time for the ternary prevaporized mixture (color scale), and trajectories of gas-phase composition during evaporation colored by simulation time. Finite- (triangles) vs zero-diffusion (circles) models. (b) Species mole fractions and (c) temperature in gas-phase, as obtained with finite- (continuous lines) and zero-diffusion models (dashed lines).

creases again because of evaporation. The increase in the gas-phase temperature also accelerates the total evaporation rate, resulting in a ~30 % faster droplet evaporation. This dynamic behavior is not observed for the finite-diffusion case, where the concentration of *n*-dodecane is not high enough to start the low-temperature mechanism during evaporation. This occurs only after the droplet has fully evaporated, and can be observed from the double inflection point of both temperature and concentration profiles.

4. Conclusions

In this work, the effect of multicomponent diffusion and preferential evaporation of surrogate fuels in a homogeneous gaseous phase was investigated. To this purpose, a numerical model was developed, describing the evolution of the liquid phase through a finite-difference approach. The combination of a Stefan–Maxwell approach for multicomponent diffusion and Peng–Robinson equation of state for the description of thermodynamic equilibrium was selected to provide a detailed representation of the relevant physical properties, while a validated skeletal mechanism (181 species, 4089 reactions) was used to describe the gas-phase chemistry in detail.

Using this model, an extended range of operating conditions, including droplet diameter and equivalence ratio, at gas-turbine relevant conditions [37] ($T_0 = 833$ K, $P = 22.1$ atm) for the 2nd-generation surrogate of a POSF 4658 Jet-A fuel was examined. It was found that the competition between fuel evaporation in the gas-phase and the subsequent cooling of the gaseous mixture determines the ignition delay time, whose behavior as a function of global equivalence ratio is non-monotonic for small diameters. More importantly, it was found that droplet ignition cannot be considered as a simple combination of droplet evaporation time and the ignition time of the prevaporized mixture. Analyzing its deviation from the sum of the two contributions allowed to identify three regions:

- A region where ignition is driven by chemical kinetics: $\tau_{ign} \approx (\tau_{evap} + \tau_{pv,ign})$ and $\tau_{evap} \ll \tau_{pv,ign}$;
- A region where ignition is controlled by evaporation: $\tau_{ign} > (\tau_{evap} + \tau_{pv,ign})$ and $\tau_{evap} \gg \tau_{pv,ign}$;
- A region where two-phase ignition significantly deviates from the ideal behavior, and droplet evaporation and ignition time scales become comparable. At these conditions, the sensitivity to preferential evaporation is most pronounced. A comparison with the autoignition map obtained with a zero-diffusivity model emphasizes significant dis-

crepancies in ignition delay times compared to a finite-diffusion model.

In summary, this work provides a useful guidance for the consideration of preferential evaporation in the modeling of two-phase combustion. This analysis can be further extended by incorporating physical processes not considered in this case. Although adding non-negligible computational complexity, the influence of gas-phase transport or slip velocity on the ignition delay time of surrogate fuels can be useful extensions of this analysis, and compounding effects can also be evaluated.

Acknowledgments

The authors gratefully acknowledge financial support through NASA with award NNX15AV04A.

Supplementary material

Supplementary material associated with this article can be found, in the online version, at [10.1016/j.proci.2016.06.052](https://doi.org/10.1016/j.proci.2016.06.052).

References

- [1] P. Dagaut, M. Cathonnet, *Prog. Energy Combust. Sci.* 32 (1) (2006) 48–92.
- [2] W.J. Pitz, C.J. Mueller, *Prog. Energy Combust. Sci.* 37 (3) (2011) 330–350.
- [3] T. Edwards, L.Q. Maurice, *J. Propuls. Power* 17 (2) (2001) 461–466.
- [4] A. Violi, S. Yan, E. Eddings, et al., *Combust. Sci. Technol.* 174 (11–12) (2002) 399–417.
- [5] A. Agosta, N. Cernansky, D. Miller, T. Faravelli, E. Ranzi, *Exp. Therm. Fluid Sci.* 28 (7) (2004) 701–708.
- [6] S. Honnet, K. Seshadri, U. Niemann, N. Peters, *Proc. Combust. Inst.* 32 (1) (2009) 485–492.
- [7] S. Dooley, S.H. Won, M. Chaos, et al., *Combust. Flame* 157 (12) (2010) 2333–2339.
- [8] S. Dooley, S.H. Won, J. Heyne, et al., *Combust. Flame* 159 (4) (2012) 1444–1466.
- [9] ASTM International, *Standard Test Method for Determination of Ignition Delay and Derived Cetane Number (DCN) of Diesel Fuel Oils by Combustion in a Constant Volume Chamber*, ASTM International, 2015, doi:10.1520/D6890-15A.
- [10] M. Tanabe, T. Bolik, C. Eigenbrod, H. Rath, J. Sato, M. Kono, in: *Symposium (International) on Combustion*, 26, Elsevier, 1996, pp. 1637–1643.
- [11] A. Cuoci, M. Mehl, G. Buzzi-Ferraris, T. Faravelli, D. Manca, E. Ranzi, *Combust. Flame* 143 (3) (2005) 211–226.
- [12] O. Moriué, M. Mikami, N. Kojima, C. Eigenbrod, *Proc. Combust. Inst.* 30 (2) (2005) 1973–1980.
- [13] T.I. Farouk, F.L. Dryer, *Combust. Flame* 161 (2) (2014) 565–581.
- [14] A. Cuoci, A. Frassoldati, T. Faravelli, E. Ranzi, *Proc. Combust. Inst.* 35 (2) (2015) 1621–1627.

- [15] A. Vié, B. Franzelli, Y. Gao, T. Lu, H. Wang, M. Ihme, *Proc. Combust. Inst.* 35 (2) (2015) 1675–1683.
- [16] A.M. Lippert, R.D. Reitz, *Technical Report 972882, SAE Technical Paper*, 1997.
- [17] Y. Ra, R.D. Reitz, *Int. J. Multiph. Flow* 35 (2) (2009) 101–117.
- [18] S. Sazhin, M. Al Qubeissi, R. Kolodnytska, A. Elwardany, R. Nasiri, M. Heikal, *Fuel* 115 (2014) 559–572.
- [19] S. Liu, J.C. Hewson, J.H. Chen, H. Pitsch, *Combust. Flame* 137 (3) (2004) 320–339.
- [20] R. Taylor, R. Krishna, *Multicomponent Mass Transfer*, vol. 2, John Wiley & Sons, 1993.
- [21] R.C. Reid, J.M. Prausnitz, B.E. Poling, *The Properties of Gases and Liquids*, McGraw Hill Book Co., New York, NY, 1987.
- [22] M. Siddiqi, K. Lucas, *Can. J. Chem. Eng.* 64 (5) (1986) 839–843.
- [23] K.K. Kuo, *Principles of Combustion*, Wiley New York et al., 1986.
- [24] J. Bellan, K. Harstad, *Int. J. Heat Mass Trans.* 30 (1) (1987) 125–136.
- [25] R.S. Miller, J. Bellan, *J. Fluid Mech.* 384 (1999) 293–338.
- [26] E. Ranzi, A. Frassoldati, R. Grana, et al., *Prog. Energy Combust. Sci.* 38 (4) (2012) 468–501.
- [27] P. Pepiot-Desjardins, H. Pitsch, *Combust. Flame* 154 (1) (2008) 67–81.
- [28] K.E. Niemeyer, C.-J. Sung, M.P. Raju, *Combust. Flame* 157 (9) (2010) 1760–1770.
- [29] A. Stagni, A. Frassoldati, A. Cuoci, T. Faravelli, E. Ranzi, *Combust. Flame* 163 (2015) 382–393.
- [30] S.S. Vasu, D.F. Davidson, Z. Hong, V. Vasudevan, R.K. Hanson, *Proc. Combust. Inst.* 32 (1) (2009) 173–180.
- [31] L. Constantinou, R. Gani, *AIChE J.* 40 (10) (1994) 1697–1710.
- [32] T.J. Bruno, L.S. Ott, B.L. Smith, T.M. Lovestead, *Anal. Chem.* 82 (3) (2009) 777–783.
- [33] M. Burger, R. Schmehl, K. Prommersberger, O. Schäfer, R. Koch, S. Wittig, *Int. J. Heat Mass Transf.* 46 (23) (2003) 4403–4412.
- [34] A. Cuoci, A. Frassoldati, T. Faravelli, E. Ranzi, *Comput. Phys. Commun.* 192 (2015) 237–264.
- [35] G. Buzzi-Ferraris, F. Manenti, *Comput. Aided Chem. Eng.* 30 (2) (2012) 1312–1316.
- [36] P. Govindaraju, M. Ihme, *Int. J. Heat Mass Transf.* (2016). (under review)
- [37] R. Lecourt, G. Linassier, G. Lavergne, in: ASME 2011 Turbo Expo: Turbine Technical Conference and Exposition, American Society of Mechanical Engineers, 2011, pp. 185–194.
- [38] A.H. Lefebvre, *Gas Turbine Combustion*, CRC Press, 1998.